NANO LETTERS

pubs.acs.org/NanoLett Letter

Ultrafast Polarization-Resolved Phonon Dynamics in Monolayer Semiconductors

Tong Lin, Xiaotong Chen, Rui Xu, Jiaming Luo, and Hanyu Zhu*

Cite This: https://doi.org/10.1021/acs.nanolett.4c02787 Read Online

ACCESS | Metrics & More | Article Recommendations | Supporting Information

ABSTRACT: Monolayer transition metal dichalcogenide semiconductors exhibit unique valleytronic properties interacting strongly with chiral phonons that break time-reversal symmetry. Here, we observed the ultrafast dynamics of linearly and circularly polarized $E'(\Gamma)$ phonons at the Brillouin zone center in single-crystalline monolayer WS_2, excited by intense, resonant, and polarization-tunable terahertz pulses and probed by time-resolved anti-Stokes Raman spectroscopy. We separated the coherent phonons producing directional sum-frequency generation from the incoherent phonon population emitting scattered photons. The longer incoherent population lifetime than what was expected from coherence lifetime indicates that inhomogeneous broadening and momentum scattering play important roles in phonon decoherence at room temperature. Meanwhile, the faster depolarization rate in circular bases than in linear bases suggests that the eigenstates are linearly polarized due to lattice anisotropy. Our results provide crucial information for improving the lifetime of chiral phonons in two-dimensional materials and potentially facilitate dynamic control of spin−orbital polarizations in quantum materials.

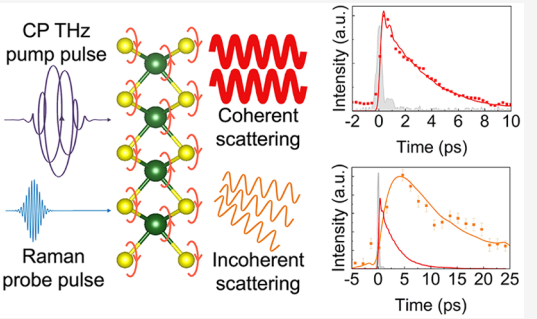

KEYWORDS: *2D monolayers, transition metal dichalcogenides, chiral phonons, time-resolved Raman spectroscopy, coherent phonon dynamics*

Two-dimensional (2D) monolayer transition metal dichalcogenides (TMDs) exhibit a wide range of intriguing electronic, optical properties and hold great potential for high-performance electronics, photonics, and optoelectronics.[1−3] Phonons in 2D TMDs couple strongly with electrons, determining the materials' key transport properties such as mobility and superconductivity.[4−6] More recently, it was discovered that chiral phonons, in which atoms rotates unidirectionally around the equilibrium position, play an important role in valleytronics, where the spin-valley-locked electrons and excitons obey selection rules during scattering processes.[7−15] Chiral phonons near the Brillouin zone center, as opposed to the zone edge valley phonons, may also exhibit unique properties such as the ability to induce spin polarization. Although zone-center chiral phonons are the coherent superposition of two degenerate modes of linearly oscillating phonons, they are fundamentally different from linear phonons due to their time-reversal symmetry (TRS) breaking.[16−23] Therefore, the dynamics of chiral phonons may be distinctive and important for manipulating asymmetric electronic and optical properties in 2D TMDs, but has not been systematically studied so far.

The dynamics of chiral phonons cannot be fully characterized by conventional spectroscopy methods. The line width of spontaneous polarization-resolved Raman scattering can be an indication of ensemble lifetime T_2^*, which include all decoherence mechanisms.[24−26] Time-resolved Raman scattering and four-wave mixing spectroscopy can obtain the incoherent population lifetime T_1 and coherent lifetime T_2^* of linearly polarized phonons in TMDs, but have not been implemented for chiral phonons.[27,28] Transient changes of excitonic transition is sensitive to the lattice displacement and can also probe coherent dynamics of phonons in monolayer TMDs,[29−31] but due to selection rule, it is nontrivial to impulsively excite coherent circularly polarized phonons with large oscillation amplitude to provide sufficiently large signal for monolayer materials.[32] Meanwhile, resonant infrared light can strongly excite coherent phonons with the same polarization and oscillation frequency, reaching an amplitude as much as a few percent of the interatomic bonds and significantly modify materials properties such as superconductivity, ferroelectricity, and topology.[33−36] The excitation mechanism should not be confused to impulsive excitation utilizing light pulses shorter than half the period of the phonons.[37] Rather, the electric field in the resonant multicycle pulses oscillate fast, but the pulses themselves can have longer

Received: June 12, 2024
Revised: August 5, 2024
Accepted: August 6, 2024

https://doi.org/10.1021/acs.nanolett.4c02787
Nano Lett. XXXX, XXX, XXX−XXX

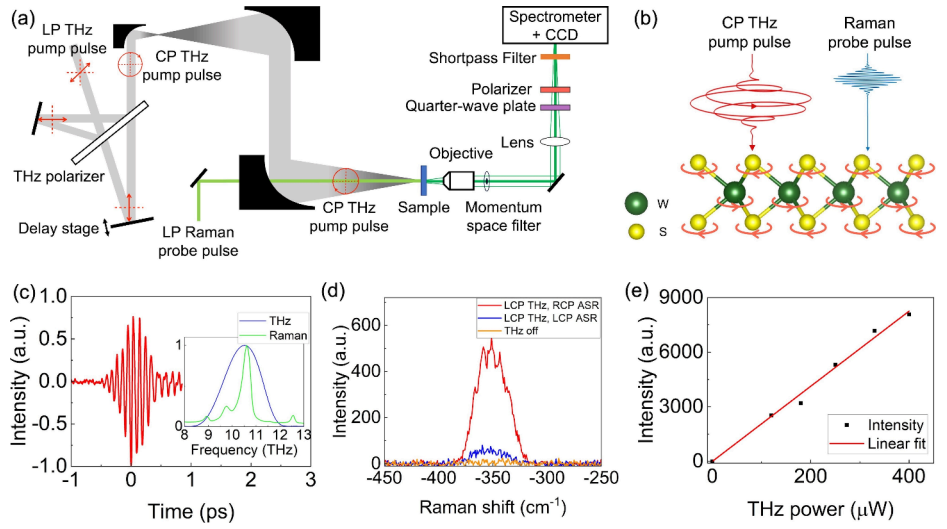

Figure 1. Resonant THz excitation of circularly polarized phonons in monolayer WS_2. (a) Schematic of the setup: The intense and broadly tunable CP THz pulse is generated by combining two cross-polarized THz beams with a phase delay of $\varphi = \pi/2$. A narrowband probe pulse with a tunable polarization generates an anti-Stokes signal from the sample in a vacuum cryostat. The coherent and incoherent scattering signals are collected by a microscope, separated by a beam block in the Fourier plane, filtered by polarization and wavelength, and detected by a spectrometer. (b) Schematic of the CP $E'(\Gamma)$ phonons in monolayer WS_2 excited by the CP THz pump pulse and optically probed. (c) The electric field of the THz pulse measured by electro-optic sampling, corresponding to a spectrum (inset blue line) centered at 10.6 THz with a bandwidth of 1.5 THz, resonant with the $E'(\Gamma)$ phonon mode in monolayer WS_2 (inset green line). (d) Anti-Stokes spectra probed at zero delay after the CP THz pump. In the absence of the THz pump, the intensity of the ASR signal is below the detection limit. With THz pump, the intensity of ASR signal increases significantly, which demonstrates that a large population of phonons has been excited. The selection rule is revealed by polarization-resolved anti-Stokes scattering. (e) Power dependence of the ASR signal intensity. The linear relationship confirms the one-photon absorption mechanism.

duration to keep driving the atomic motion in phase. This excitation mechanism has been validated by multiple experimental and theoretical studies before.[20,34] The phonon number in a specific mode created by infrared excitation is much higher than any other methods, including ultrafast heating and impulsive/stimulated Raman scattering, and thus may enable detailed studies of nonlinear phononics and phonon-mediated electronic/spin dynamics with high sensitivity at the nanoscale.[20,38−45]

Here we directly resonantly excited coherent chiral $E'(\Gamma)$ phonons in monolayer WS_2 by intense circularly polarized (CP) terahertz (THz) photons. We then probed the dynamics of both LP and CP phonons through time- and polarization-resolved anti-Stokes Raman (ASR) scattering. The strong ASR signal benefited from the large phonon amplitude excited by the intense THz pulses, and its coherence contains phonons' phase information. Importantly, time-resolved spectroscopy allows us to distinguish the dynamics of almost degenerate $E'(\Gamma)$ and 2LA modes that overlap in spontaneous Raman spectrum. Moreover, we measured the properties of incoherent and coherent phonons independently utilizing the different angular distributions of their scattering signals. We found that $E'(\Gamma)$ phonons in monolayer WS_2 can lose coherence without losing energy, since the population lifetime is much longer than half of the coherence lifetime at room temperature. The coherence lifetime increases by almost half at 20 K, but less than that in MoS_2, possibly due to the resonance decay from $E'(\Gamma)$ to 2LA. When decomposing the phonons into linear and circular bases, we observed longer coherence lifetime in linear bases, meaning that they are more likely the eigenstates of the $E'(\Gamma)$ mode, whose degeneracy might have been broken by lattice anisotropy. Due to the lack of rotational symmetry and angular momentum conservation, scattering almost always reduces chiral population, such that the incoherent population lifetime of CP phonons is not different from half of the coherence lifetime. Our findings are crucial steps toward understanding and controlling the quantum properties of chiral phonons that potentially couple with spintronic, excitonic, and valleytronic properties in 2D semiconductors.

Figure 1a illustrates the resonant THz-pump, Raman-probe hyperspectral microscopy with momentum resolution for exfoliated single-crystalline monolayer WS_2 (Supporting Information). The field strength of the CP THz pulse is about 1 MV/cm, which excites CP phonons (Figure 1b) with a coherent displacement more than 2 orders of magnitude larger than what could be achieved by nonlinear mixing in previous studies.[32] The pulse centered at 10.6 THz with a 1.5 THz bandwidth resonates with the circularly polarized $E'(\Gamma)$ phonon mode in monolayer WS_2 (Figure 1c), which is both IR and Raman active, as well as the two-phonon process 2LA at the peak of the density of state of the longitudinal acoustic phonons.[46] The phonon dynamics probed by time-resolved anti-Stokes Raman (ASR) scattering I_{AS} is proportional to the phonon population.[47−49] The frequency of the phonons is thus directly obtained in the spectral domain, instead of by Fourier-transforming an oscillating signal in the time domain. The temporal resolution of the spectrally resolved signal is limited to the duration of the probe pulse (0.5 ps), which effectively performs a wavelet transformation to the photon displacement as shown in the next section. At room temperature, the intensity of ASR signal without THz pump was beyond the detection limit of our setup due to low thermal population and small probe power, but under the THz pump the strong signal indicates efficient and linear excitation of chiral phonons (Figure 1d and 1e). We verified the chirality of the phonons according to the pseudoangular momentum conservation: the incident photons and the phonons must have the same circular polarization, and the scattered photons must have the opposite

https://doi.org/10.1021/acs.nanolett.4c02787
Nano Lett. XXXX, XXX, XXX−XXX

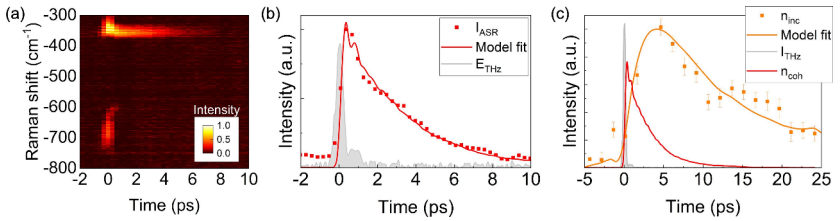

Figure 2. Coherent and incoherent phonon dynamics revealed by time-resolved anti-Stokes Raman scattering. (a) Temporal evolution of the ASR spectra at room temperature. The feature centered around 350 cm^{-1} mainly arises from the $E'(\Gamma)$ phonon modes, and the feature centered around 700 cm^{-1} comes from the sum frequency generation with the THz overtone. Integrating the spectral component of the phonon modes yields (b) the dynamics of coherent phonons. The experimental ASR intensity (square) fits well with the model (eq 3, red solid line) using a damping rate of 0.99 ± 0.06 cm^{-1}, corresponding to a spatiotemporal dephasing lifetime of 5.4 ± 0.3 ps for the coherent phonons. Gray curve shows the amplitude of the electric field of the THz pump pulse. (c) Blocking the coherent component of ASR gives a fitted lifetime of 6.1 ± 0.3 ps (eq 4, yellow solid line) at room temperature for incoherent phonon population (square), which is generated by the intensity of both the THz pump $c_1 I_{THz}(t)$ (gray curve) and the coherent phonon population $c_2 n_{coh}(t)$ (red curve).

polarization.[50] Here the incident probe is linearly polarized and can be decomposed into a mixture of equal amounts of left-circularly polarized (LCP) photons and right-circularly polarized (RCP) photons to scatter with phonons in both polarizations.

With the coherent resonant excitation of phonons in monolayers, we first differentiated the time-resolved decoherence and population relaxation dynamics, providing more information than what can be deduced by the line width measurements from Raman, X-ray, and neutron scattering.[51−53] Figure 2a shows the THz pump-induced anti-Stokes scattering signal, spectrally shifted with respect to the center wavenumber of the probe pulse, as a function of delay time at room temperature. Here both the THz pump pulse and the Raman probe pulse here were not polarized, and signals in all polarizations and scattering angles were collected. The nonequilibrium dynamics of phonons excited by THz pump pulse consists simultaneously of coherent and incoherent contributions (Supporting Information Sections 3 and 4).[54] Because both the THz pump and Raman probe pulses are normal incident, the coherent phonons and the light scattered by them are in-phase. Therefore, the exiting coherent signal is also normal to the surface and propagates collinearly with the incoming pulses. In contrast, the incoherent phonons are random in phase and the scattered light is in all directions. Without any momentum filter in the back-focal plane, the integrated intensity of the ASR peak around 350 cm^{-1} is dominated by the dynamics of the coherent $E'(\Gamma)$ phonons. Under such conditions, the Raman probe is equivalent to vibrational sum-frequency generation (SFG) spectroscopy widely used in studying vibrational states of molecules.[55] The physical process can be described by a phenomenological two-step model.[56] In step one, the THz excitation centered around a low frequency of Ω initiates the coherent ionic polarization $P_j(\Omega) \propto 1/(\Omega_j - \Omega - i\Gamma_j)$ from the j-th phonon mode with a center frequency of Ω_j, as well as a nonresonant electronic polarization. In step two, the polarization is upconverted to a coherent optical emission signal centered around $\omega_0+\Omega_j$ by a visible pulse at a high frequency ω_0 and delayed by τ with respect to the THz excitation.

The damping rate Γ_j may account for several possible decoherence mechanisms, and we adopt the symbols from spin resonance spectroscopy for our discussion.[57] Γ_1 defines population relaxation, usually caused by optical phonons splitting into acoustic phonons. Correspondingly, the population lifetime from incoherent ASR is determined as $T_1 = 1/4\pi\Gamma_1$. Γ^* denotes nonlocal dephasing within the measurement volume such as inhomogeneous broadening by static strain or soft out-of-plane acoustic (ZA) phonons that changes the momentum of phonons but nearly preserves their energy. It can be extracted by the "spatial decoherence lifetime" of unpolarized but spatially coherent phonons, $T^* = 1/2\pi(\Gamma_1+\Gamma^*)$. Lastly, Γ_2 refers to depolarization due to local coupling. The ensemble decoherence lifetime includes contributions from all loss mechanisms $T_2^* = 1/2\pi(\Gamma_1+\Gamma_2+\Gamma^*)$, which can often be inferred from the inverse of the half width at half-maximum (HWHM) of the spontaneous Raman spectrum, but could be measured more reliably by time-domain polarization-resolved spectroscopy for 2D materials with long phonon lifetimes. Although T_2^* in monolayers is likely shorter due to substrate effect, the bulk values (5 ps at room temperature, 7 ps at cryogenic temperature) obtained from previous high-resolution Raman measurements provides good estimates of the lower bound of our following measurements of phonon dynamics.[58] Overall, these lifetimes are expected to follow the relation $2T_1 \geq T^* \geq T_2^*$, and can be independently measured to extract Γ_1, Γ_2, and Γ^*, which unveils different decoherence mechanisms and mitigation routes.

Fitting the experimentally measured ASR intensity (Figure 2b) by the model (eq S1−S3) gives a damping rate $\Gamma_1+\Gamma^* = 0.99 \pm 0.06$ cm^{-1}, or a spatial coherence lifetime $T_{2,295K}^* = 5.4 \pm 0.3$ ps, for the $E'(\Gamma)$ phonon at room temperature. Since we did not differentiate the polarization of the signal, depolarization Γ_2 was not included in the decoherence process. For 2LA mode, the lifetime at room temperature deduced from Raman line width is close to the duration of THz pump pulse (0.4 ps). Therefore, 2LA decays much faster than E′(Γ) mode and is not distinguishable from the nonresonant response.

The incoherent dynamics was measured by blocking the spatially coherent signal in the momentum space. The dynamics is qualitatively different from that of the unblocked beam, corroborating that the incoherent scattering dominated the signal despite being 2 orders of magnitude weaker than coherent SFG. The incoherent population rises from both direct THz excitation and momentum scattering of coherent phonons, and then decays exponentially with a constant of population lifetime $T_{1,295K} = 1/4\pi\Gamma_1 = 6.1 \pm 0.3$ ps (fitting from eq S4). We found that the incoherent population lifetime obtained from our study is longer than the previous reported value of 4.3 ps in CVD grown monolayer WS_2[27] and it agrees well with the results predicted by first-principles calculations.[59]

https://doi.org/10.1021/acs.nanolett.4c02787
Nano Lett. XXXX, XXX, XXX−XXX

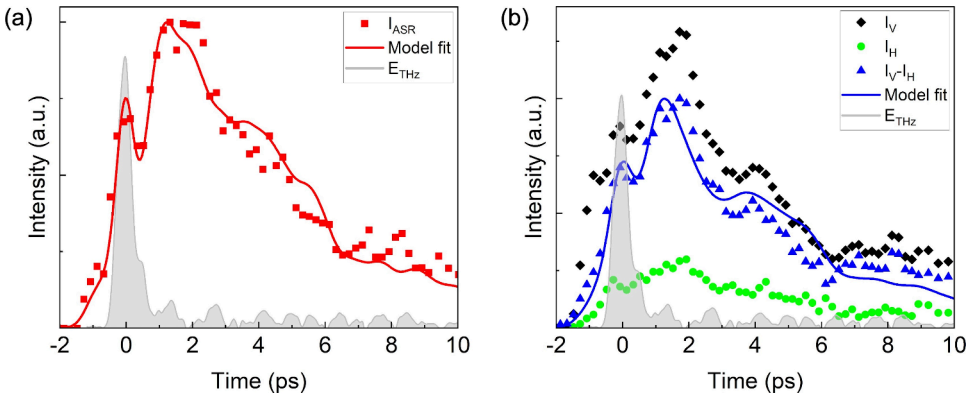

Figure 3. Coherence dynamics revealed by polarization-resolved anti-Stokes Raman scattering in linear bases. (a) Spatial decoherence measured under the same optical setup as Figure 2a but at 20 K, showing an extended lifetime of 7.9 ± 0.6 ps. (b) Depolarization dynamics observed from the scattered coherent Raman signal in linear polarization bases H and V. Both the THz pump pulses and the Raman probe pulses are horizontally polarized along the crystal's zigzag direction. The depolarization lifetime of the $E'(\Gamma)$ phonon mode is 8.6 ± 0.6 ps, equal to the spatial decoherence lifetime within error, indicating a negligible contribution from any depolarization channels that preserves momentum.

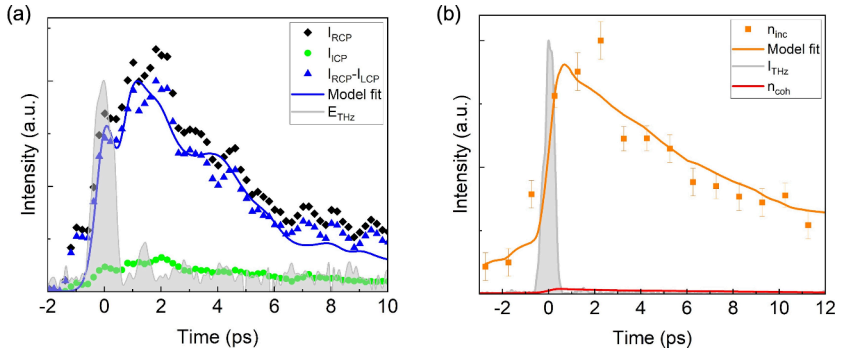

Figure 4. Chirality dynamics revealed by polarization-resolved anti-Stokes Raman scattering in CP bases. (a) Both the THz pump pulse and the Raman probe pulse are LCP. Output signal was detected in CP bases with a coherence lifetime of 7.2 ± 0.7 ps. (b) The chirality lifetime of 4.0 ± 0.4 ps of the incoherent optical phonons (yellow squares) is measured by blocking the signal from coherent phonons, which make only a small contribution (red curve) to the incoherent phonon dynamics.

This is most likely due to fewer defects in mechanical exfoliated samples than CVD samples,[60] leading to longer population lifetime. Notably, T_1 is significantly longer than $T^*/2$ and $T_2^*/2$, indicating that inhomogeneous broadening and the scattering from acoustic phonons are important factors for phonon decoherence at room temperature. This is consistent with theoretical calculations that the four-phonon scattering process is more prominent at higher temperatures.[58,61,62]

To understand the coherence dynamics of polarized phonons, which is crucial for ultrafast lattice control of quantum materials, we measured the depolarization dynamics of linearly polarized $E'(\Gamma)$ phonons with the help of Raman selection rules in monolayer WS_2. Theory predicts that in cryogenic temperatures, spatial decoherence from scattering with acoustic phonons should be suppressed compared to room temperature, potentially allowing pure depolarization to be observed. Thus, we cooled down the monolayer WS_2 sample in a cryostat to reach a base temperature of 20 K. We first measured the spatial dephasing lifetime of the coherent phonon under the same optical configurations as those described previously to obtain Figure 2b, and fitted the experimental data using the same model, as shown in Figure 3a. The dynamics is complicated by the increasing response of 2LA mode due to stronger excitonic enhancement at low temperatures.[58] In typical spontaneous Raman scattering, it is quite challenging to separate 2LA and $E'(\Gamma)$ peaks especially when the line width approaches the instrumental limit. But in time-resolved measurements they are distinguishable from decay dynamics. Due to different selection rules, 2LA and $E'(\Gamma)$ can destructively interfere with each other, resulting in an apparent "rising feature" that actually corresponds to the relaxation of 2LA, similar to the "quantum beats" previously observed in molecular SFG spectra.[63]

From Figure 3a, we observed that the spatial dephasing lifetime of the $E'(\Gamma)$ phonon is indeed extended to $T_{2K}^* = 7.9 \pm 0.6$ ps, corresponding to a HWHM of 0.67 cm^{-1}. The temperature dependence is not as sharp as that of the $E'(\Gamma)$ mode in MoS_2, which increases to almost three times at 15 K,[28] possibly due to the nearly resonant down-conversion from $E'(\Gamma)$ to 2LA that warrant further theoretical and experimental investigations. The effective coherence lifetime of 2LA phonon is 1.1 ± 0.4 ps, corresponding to a HWHM of 4.8 cm^{-1} representing the width of density of states for all possible two-phonon combinations. Both values are consistent with a high-resolution Raman study of bulk WS_2 at 3.6 K using multi-Lorentzian fitting.[58] Our time-resolved method is thus particularly suitable for studying phonon modes with longer lifetime, when the intrinsic narrow line width is shadowed by the instrument broadening or large unwanted features nearby in conventional Raman spectroscopy.

https://doi.org/10.1021/acs.nanolett.4c02787
Nano Lett. XXXX, XXX, XXX−XXX

We then probed the dynamics of depolarization at 20 K in linear bases. The THz pump pulses were set to horizontal polarization to excite horizontally polarized (H) $E'(\Gamma)$ phonons, i.e., atoms displacing along the zigzag direction of the lattice, and the Raman probe pulses were also horizontally polarized. According to the selection rule, H phonons scatter light into vertical polarization I_V. Meanwhile, the vertically polarized (V) phonon population can arise due to polarization decoherence, and its dynamics can be distinguished from that of H phonons by selecting the horizontally polarized signal I_H. Figure 3b depicts the temporal evolution of I_V, I_H, as well as their difference I_V-I_H. Fitting the temporal evolution of I_V-I_H gives a lifetime in LP bases is 8.6 ± 0.6 ps, no shorter than the spatial coherence lifetime T^*_{20K} without polarization resolution. The fact that we did not observe additional depolarization processes indicates that linear bases are reasonable eigenstates of the $E'(\Gamma)$ under our experimental conditions, and there is no observable TRS breaking scattering that couples the linear modes.

Finally, we measured the "chirality" dynamics of 2D phonons that can manipulate the TRS of materials. The $E'(\Gamma)$ phonon mode can be written in left and right CP bases, which only scatters light in the same circular polarization into oppositely polarized ASR signal. Here, we utilized LCP THz pump pulses to excite LCP phonons, and linearly polarized Raman pulses consisting of LCP and RCP components to probe the phonons. The scattered light intensity I_{RCP} and I_{LCP} are proportional to n_{LCP} and n_{RCP}, respectively (Figure 1c). Figure 4a displays the temporal evolution of I_{RCP}, I_{LCP}, as well as their difference I_{RCP}-I_{LCP}, from which we calculated a spatial coherence lifetime in CP bases is 7.2 ± 0.7 ps. The lifetime in CP bases is shorter than that in LP bases, indicating a nonzero Γ_2. The results suggest that chirality is likely more susceptible to scattering processes than linearity for $E'(\Gamma)$. This is not always obvious, since scattering with low-energy acoustic phonons or free electrons/holes should approximately obey pseudoangular momentum conservation in a perfectly rotation-symmetric crystal.[64] Therefore, it appears that local lattice anisotropy, such as strain that breaks the 3-fold symmetry, makes a non-negligible contribution to the loss of chirality without necessarily affecting the linearity of the phonons. This is consistent with the previous conclusion that linear bases are better eigenstates of $E'(\Gamma)$ phonons in our materials produced by mechanical exfoliation. Thus, $T^{*,CP}_{20K}$ includes the polarization dephasing process and is a reasonable approximation of $T^*_{2,20K}$. We also checked the dynamics of incoherent circularly polarized phonons by blocking the coherent SFG in the momentum space (Figure 4b). Using eq 4, we determined the phonon chirality lifetime $T^{CP}_{1,\,20K}$ = 4.0 ± 0.4 ps ≅ $T^*_{2,\,20K}/2$. This result, i.e., $2T_1 = T_2^*$ for CP phonons, is in stark contrast to nonpolarized measurements (Figure 2), again demonstrating that there exist scattering channels that nearly conserve energy but do not conserve pseudoangular momentum due to broken 3-fold rotational symmetry. At cryogenic temperature, the probability of momentum scattering greatly reduced because of a lower population of thermal acoustic phonons, whose contribution to the incoherent phonon dynamics (red curve in Figure 4b) is almost negligible. Therefore, the rising incoherent phonon population is sharper compared to room temperature. Further theoretical and experimental research may help to quantify the relation between lattice symmetry breaking and loss of angular momentum in phonon scattering. Our results on chirality dynamics for the first time are useful for engineering chiral phonons, as well as future works to extend coherence lifetime for nonlinear and quantum phononics in low-dimensional materials.

In summary, we have performed a systematic study of coherent and incoherent dynamics of infrared and Raman active $E'(\Gamma)$ phonons in monolayer WS_2. A large population of single mode coherent phonons in linear and circular polarizations has been efficiently generated by intense resonant THz pump excitation. This is not achievable by thermal or optical impulsive excitations in previous studies. The strong phonon excitation enabled time- and polarization-resolved coherent and incoherent ASR microscopy in mechanically nanoscale exfoliated single crystals for the first time. We quantified the population lifetime, spatial dephasing lifetime, depolarization lifetime, and chirality lifetime by momentum- and polarization-selection, and differentiated a few possible decoherence mechanisms to help improve the phonon coherence in the future. We found that spatial decoherence rate Γ^* drops to negligible at cryogenic temperatures, but the polarization decoherence rate Γ_2 remains finite, suggesting the possibility of anisotropic coupling due to static strain, which might be mitigated during the fabrication process. The information on coherence and chirality dynamics is essential for ultrafast, on-demand, and noninvasive lattice engineering of spin and orbital degrees of freedom in nonmagnetic quantum materials. Moreover, the methodology is generally applicable for studying phonon dynamics in noncentrosymmetric nanomaterials to yield more details than what can be obtained from the line width measurements in conventional Raman or infrared spectroscopy. It may also be applicable for revealing the dynamics of zone-edge valley chiral phonons, as well as localized defect vibrations, which have weak Raman scattering that can be amplified by resonance excitation. Furthermore, the coherent momentum microscopy may be useful in analyzing the spatial inhomogeneity of lattices and phonon diffusion.

■ ASSOCIATED CONTENT

Supporting Information

The Supporting Information is available free of charge at https://pubs.acs.org/doi/10.1021/acs.nanolett.4c02787.

Details of experimental setup, materials characterization, and modeling of phonon dynamics (PDF)

■ AUTHOR INFORMATION

Corresponding Author

Hanyu Zhu − *Department of Materials Science and NanoEngineering, Rice University, Houston, Texas 77005, United States;* orcid.org/0000-0003-3376-5352; Email: Hanyu.Zhu@rice.edu

Authors

Tong Lin − *Department of Materials Science and NanoEngineering, Rice University, Houston, Texas 77005, United States*

Xiaotong Chen − *Department of Materials Science and NanoEngineering, Rice University, Houston, Texas 77005, United States*

Rui Xu − *Department of Materials Science and NanoEngineering, Rice University, Houston, Texas 77005, United States;* orcid.org/0000-0002-7072-1976

https://doi.org/10.1021/acs.nanolett.4c02787
Nano Lett. XXXX, XXX, XXX−XXX

Jiaming Luo − *Department of Materials Science and NanoEngineering, Rice University, Houston, Texas 77005, United States;* orcid.org/0009-0007-8362-9558

Complete contact information is available at: https://pubs.acs.org/10.1021/acs.nanolett.4c02787

Notes

The authors declare no competing financial interest.

■ ACKNOWLEDGMENTS

This work is supported by the U.S. National Science Foundation (DMR-2240106) and Robert A. Welch Foundation (C-2128).

■ REFERENCES

(1) Wang, Q. H.; Kalantar-Zadeh, K.; Kis, A.; Coleman, J. N.; Strano, M. S. Electronics and Optoelectronics of Two-Dimensional Transition Metal Dichalcogenides. *Nat. Nanotechnol.* **2012**, *7* (11), 699−712.

(2) Manzeli, S.; Ovchinnikov, D.; Pasquier, D.; Yazyev, O. V.; Kis, A. 2D Transition Metal Dichalcogenides. *Nat. Rev. Mater.* **2017**, *2* (8), 17033.

(3) Choi, W.; Choudhary, N.; Han, G. H.; Park, J.; Akinwande, D.; Lee, Y. H. Recent Development of Two-Dimensional Transition Metal Dichalcogenides and Their Applications. *Mater. Today* **2017**, *20* (3), 116−130.

(4) Kaasbjerg, K.; Thygesen, K. S.; Jacobsen, K. W. Phonon-Limited Mobility in n-Type Single-Layer MoS2 from First Principles. *Phys. Rev. B* **2012**, *85* (11), 115317.

(5) Kang, M.; Jung, S. W.; Shin, W. J.; Sohn, Y.; Ryu, S. H.; Kim, T. K.; Hoesch, M.; Kim, K. S. Holstein Polaron in a Valley-Degenerate Two-Dimensional Semiconductor. *Nat. Mater.* **2018**, *17* (8), 676−680.

(6) Lu, J. M.; Zheliuk, O.; Leermakers, I.; Yuan, N. F. Q.; Zeitler, U.; Law, K. T.; Ye, J. T. Evidence for Two-Dimensional Ising Superconductivity in Gated MoS2. *Science* **2015**, *350* (6266), 1353−1357.

(7) Zhang, L.; Niu, Q. Chiral Phonons at High-Symmetry Points in Monolayer Hexagonal Lattices. *Phys. Rev. Lett.* **2015**, *115* (11), 115502.

(8) Chen, S.-Y.; Zheng, C.; Fuhrer, M. S.; Yan, J. Helicity-Resolved Raman Scattering of MoS2, MoSe2, WS2, and WSe2 Atomic Layers. *Nano Lett.* **2015**, *15* (4), 2526−2532.

(9) Zhu, H.; Yi, J.; Li, M.-Y.; Xiao, J.; Zhang, L.; Yang, C.-W.; Kaindl, R. A.; Li, L.-J.; Wang, Y.; Zhang, X. Observation of Chiral Phonons. *Science* **2018**, *359* (6375), 579−582.

(10) Chen, H.; Zhang, W.; Niu, Q.; Zhang, L. Chiral Phonons in Two-Dimensional Materials. *2D Mater.* **2019**, *6* (1), 012002.

(11) He, M.; Rivera, P.; Van Tuan, D.; Wilson, N. P.; Yang, M.; Taniguchi, T.; Watanabe, K.; Yan, J.; Mandrus, D. G.; Yu, H.; Dery, H.; Yao, W.; Xu, X. Valley Phonons and Exciton Complexes in a Monolayer Semiconductor. *Nat. Commun.* **2020**, *11* (1), 618.

(12) Liu, E.; van Baren, J.; Taniguchi, T.; Watanabe, K.; Chang, Y.-C.; Lui, C. H. Valley-Selective Chiral Phonon Replicas of Dark Excitons and Trions in Monolayer WS e 2. *Phys. Rev. Res.* **2019**, *1* (3), 032007.

(13) Li, Z.; Wang, T.; Jin, C.; Lu, Z.; Lian, Z.; Meng, Y.; Blei, M.; Gao, M.; Taniguchi, T.; Watanabe, K.; Ren, T.; Cao, T.; Tongay, S.; Smirnov, D.; Zhang, L.; Shi, S.-F. Momentum-Dark Intervalley Exciton in Monolayer Tungsten Diselenide Brightened via Chiral Phonon. *ACS Nano* **2019**, *13* (12), 14107−14113.

(14) Chen, X.; Lu, X.; Dubey, S.; Yao, Q.; Liu, S.; Wang, X.; Xiong, Q.; Zhang, L.; Srivastava, A. Entanglement of Single-Photons and Chiral Phonons in Atomically Thin WSe 2. *Nat. Phys.* **2019**, *15* (3), 221−227.

(15) Helmrich, S.; Sampson, K.; Huang, D.; Selig, M.; Hao, K.; Tran, K.; Achstein, A.; Young, C.; Knorr, A.; Malic, E.; Woggon, U.; Owschimikow, N.; Li, X. Phonon-Assisted Intervalley Scattering Determines Ultrafast Exciton Dynamics in MoSe 2 Bilayers. *Phys. Rev. Lett.* **2021**, *127* (15), 157403.

(16) Juraschek, D. M.; Spaldin, N. A. Orbital Magnetic Moments of Phonons. *Phys. Rev. Mater.* **2019**, *3* (6), 064405.

(17) Geilhufe, R. M. Dynamic Electron-Phonon and Spin-Phonon Interactions Due to Inertia. *Phys. Rev. Res.* **2022**, *4* (1), L012004.

(18) Ishito, K.; Mao, H.; Kousaka, Y.; Togawa, Y.; Iwasaki, S.; Zhang, T.; Murakami, S.; Kishine, J.; Satoh, T. Truly Chiral Phonons in α-HgS. *Nat. Phys.* **2023**, *19*, 35−39.

(19) Ueda, H.; García-Fernández, M.; Agrestini, S.; Romao, C. P.; van den Brink, J.; Spaldin, N. A.; Zhou, K.-J.; Staub, U. Chiral Phonons in Quartz Probed by X-Rays. *Nature* **2023**, *618* (7967), 946−950.

(20) Luo, J.; Lin, T.; Zhang, J.; Chen, X.; Blackert, E. R.; Xu, R.; Yakobson, B. I.; Zhu, H. Large Effective Magnetic Fields from Chiral Phonons in Rare-Earth Halides. *Science* **2023**, *382* (6671), 698−702.

(21) Chaudhary, S.; Juraschek, D. M.; Rodriguez-Vega, M.; Fiete, G. A. Giant Effective Magnetic Moments of Chiral Phonons from Orbit-Lattice Coupling. *arXiv Preprint*, 2023. DOI: 10.48550/arXiv.2306.11630.

(22) Basini, M.; Pancaldi, M.; Wehinger, B.; Udina, M.; Tadano, T.; Hoffmann, M. C.; Balatsky, A. V.; Bonetti, S. Terahertz Electric-Field Driven Dynamical Multiferroicity in $SrTiO_3$. *arXiv Preprint*, 2022. DOI: 10.48550/arXiv.2210.01690.

(23) Davies, C. S.; Fennema, F. G. N.; Tsukamoto, A.; Razdolski, I.; Kimel, A. V.; Kirilyuk, A. Phononic Switching of Magnetization by the Ultrafast Barnett Effect. *arXiv Preprint*, 2023. DOI: 10.48550/arXiv.2305.11551

(24) Fischer, S. F.; Laubereau, A. Dephasing Processes of Molecular Vibrations in Liquids. *Chem. Phys. Lett.* **1975**, *35* (1), 6−12.

(25) Yin, T.; Ulman, K. A.; Liu, S.; Granados del Águila, A.; Huang, Y.; Zhang, L.; Serra, M.; Sedmidubsky, D.; Sofer, Z.; Quek, S. Y.; Xiong, Q. Chiral Phonons and Giant Magneto-Optical Effect in $CrBr_3$ 2D Magnet. *Adv. Mater.* **2021**, *33* (36), 2101618.

(26) Du, L.; Tang, J.; Zhao, Y.; Li, X.; Yang, R.; Hu, X.; Bai, X.; Wang, X.; Watanabe, K.; Taniguchi, T.; Shi, D.; Yu, G.; Bai, X.; Hasan, T.; Zhang, G.; Sun, Z. Lattice Dynamics, Phonon Chirality, and Spin−Phonon Coupling in 2D Itinerant Ferromagnet Fe_3GeTe_2. *Adv. Funct. Mater.* **2019**, *29* (48), 1904734.

(27) Han, S.; Boguschewski, C.; Gao, Y.; Xiao, L.; Zhu, J.; van Loosdrecht, P. H. M. Incoherent Phonon Population and Exciton-Exciton Annihilation Dynamics in Monolayer WS_2 Revealed by Time-Resolved Resonance Raman Scattering. *Opt. Express* **2019**, *27* (21), 29949−29961.

(28) Sun, L.; Kumar, P.; Liu, Z.; Choi, J.; Fang, B.; Roesch, S.; Tran, K.; Casara, J.; Priego, E.; Chang, Y.-M.; Moody, G.; Silverman, K. L.; Lorenz, V. O.; Scheibner, M.; Luo, T.; Li, X. Phonon Dephasing Dynamics in MoS_2. *Nano Lett.* **2021**, *21* (3), 1434−1439.

(29) Jeong, T. Y.; Jin, B. M.; Rhim, S. H.; Debbichi, L.; Park, J.; Jang, Y. D.; Lee, H. R.; Chae, D.-H.; Lee, D.; Kim, Y.-H.; Jung, S.; Yee, K. J. Coherent Lattice Vibrations in Mono- and Few-Layer WSe_2. *ACS Nano* **2016**, *10* (5), 5560−5566.

(30) Bassman, L.; Krishnamoorthy, A.; Kumazoe, H.; Misawa, M.; Shimojo, F.; Kalia, R. K.; Nakano, A.; Vashishta, P. Electronic Origin of Optically-Induced Sub-Picosecond Lattice Dynamics in MoSe2-Monolayer. *Nano Lett.* **2018**, *18* (8), 4653−4658.

(31) Trovatello, C.; Miranda, H. P. C.; Molina-Sánchez, A.; Borrego-Varillas, R.; Manzoni, C.; Moretti, L.; Ganzer, L.; Maiuri, M.; Wang, J.; Dumcenco, D.; Kis, A.; Wirtz, L.; Marini, A.; Soavi, G.; Ferrari, A. C.; Cerullo, G.; Sangalli, D.; Conte, S. D. Strongly Coupled Coherent Phonons in Single-Layer MoS_2. *ACS Nano* **2020**, *14* (5), 5700−5710.

(32) Wefers, M. M.; Kawashima, H.; Nelson, K. A. Optical Control over Two-Dimensional Lattice Vibrational Trajectories in Crystalline Quartz. *J. Chem. Phys.* **1998**, *108* (24), 10248−10255.

(33) Merlin, R. Generating Coherent THz Phonons with Light Pulses. *Solid State Commun.* **1997**, *102* (2), 207−220.

(34) Först, M.; Manzoni, C.; Kaiser, S.; Tomioka, Y.; Tokura, Y.; Merlin, R.; Cavalleri, A. Nonlinear Phononics as an Ultrafast Route to Lattice Control. *Nat. Phys.* **2011**, *7* (11), 854−856.
(35) von Hoegen, A.; Mankowsky, R.; Fechner, M.; Först, M.; Cavalleri, A. Probing the Interatomic Potential of Solids with Strong-Field Nonlinear Phononics. *Nature* **2018**, *555* (7694), 79−82.
(36) Disa, A. S.; Fechner, M.; Nova, T. F.; Liu, B.; Först, M.; Prabhakaran, D.; Radaelli, P. G.; Cavalleri, A. Polarizing an Antiferromagnet by Optical Engineering of the Crystal Field. *Nat. Phys.* **2020**, *16* (9), 937−941.
(37) Yan, Y.; Gamble, E. B.; Nelson, K. A. Impulsive Stimulated Scattering: General Importance in Femtosecond Laser Pulse Interactions with Matter, and Spectroscopic Applications. *J. Chem. Phys.* **1985**, *83* (11), 5391−5399.
(38) Mankowsky, R.; Subedi, A.; Först, M.; Mariager, S. O.; Chollet, M.; Lemke, H. T.; Robinson, J. S.; Glownia, J. M.; Minitti, M. P.; Frano, A.; Fechner, M.; Spaldin, N. A.; Loew, T.; Keimer, B.; Georges, A.; Cavalleri, A. Nonlinear Lattice Dynamics as a Basis for Enhanced Superconductivity in YBa2Cu3O6.5. *Nature* **2014**, *516* (7529), 71−73.
(39) Nicoletti, D.; Cavalleri, A. Nonlinear Light−Matter Interaction at Terahertz Frequencies. *Adv. Opt. Photonics* **2016**, *8* (3), 401.
(40) Nova, T. F.; Cartella, A.; Cantaluppi, A.; Först, M.; Bossini, D.; Mikhaylovskiy, R. V.; Kimel, A. V.; Merlin, R.; Cavalleri, A. An Effective Magnetic Field from Optically Driven Phonons. *Nat. Phys.* **2017**, *13* (2), 132−136.
(41) Salén, P.; Basini, M.; Bonetti, S.; Hebling, J.; Krasilnikov, M.; Nikitin, A. Y.; Shamuilov, G.; Tibai, Z.; Zhaunerchyk, V.; Goryashko, V. Matter Manipulation with Extreme Terahertz Light: Progress in the Enabling THz Technology. *Phys. Rep.* **2019**, *836*−*837*, 1−74.
(42) Tauchert, S. R.; Volkov, M.; Ehberger, D.; Kazenwadel, D.; Evers, M.; Lange, H.; Donges, A.; Book, A.; Kreuzpaintner, W.; Nowak, U.; Baum, P. Polarized Phonons Carry Angular Momentum in Ultrafast Demagnetization. *Nature* **2022**, *602* (7895), 73−77.
(43) Frischwasser, K.; Cohen, K.; Kher-Alden, J.; Dolev, S.; Tsesses, S.; Bartal, G. Real-Time Sub-Wavelength Imaging of Surface Waves with Nonlinear near-Field Optical Microscopy. *Nat. Photonics* **2021**, *15* (6), 442−448.
(44) Niemann, R.; Mueller, N. S.; Wasserroth, S.; Lu, G.; Wolf, M.; Caldwell, J. D.; Paarmann, A. Spectroscopic and Interferometric Sum-Frequency Imaging of Strongly Coupled Phonon Polaritons in SiC Metasurfaces. *arXiv Preprint*, 2023. http://arxiv.org/abs/2311.13284
(45) Lin, T.; Xu, R.; Chen, X.; Guan, Y.; Yao, M.; Zhang, J.; Li, X.; Zhu, H. Subwavelength, Phase-Sensitive Microscopy of Third-Order Nonlinearity in Terahertz Frequencies. *ACS Photonics* **2024**, *11*, 33.
(46) Berkdemir, A.; Gutiérrez, H. R.; Botello-Méndez, A. R.; Perea-López, N.; Elías, A. L.; Chia, C.-I.; Wang, B.; Crespi, V. H.; López-Urías, F.; Charlier, J.-C.; Terrones, H.; Terrones, M. Identification of Individual and Few Layers of WS2 Using Raman Spectroscopy. *Sci. Rep.* **2013**, *3* (1), 1755.
(47) Song, D.; Wang, F.; Dukovic, G.; Zheng, M.; Semke, E. D.; Brus, L. E.; Heinz, T. F. Direct Measurement of the Lifetime of Optical Phonons in Single-Walled Carbon Nanotubes. *Phys. Rev. Lett.* **2008**, *100* (22), 225503.
(48) Yan, H.; Song, D.; Mak, K. F.; Chatzakis, I.; Maultzsch, J.; Heinz, T. F. Time-Resolved Raman Spectroscopy of Optical Phonons in Graphite: Phonon Anharmonic Coupling and Anomalous Stiffening. *Phys. Rev. B* **2009**, *80* (12), 121403.
(49) Kang, K.; Abdula, D.; Cahill, D. G.; Shim, M. Lifetimes of Optical Phonons in Graphene and Graphite by Time-Resolved Incoherent Anti-Stokes Raman Scattering. *Phys. Rev. B* **2010**, *81* (16), 165405.
(50) Chen, S.-Y.; Zheng, C.; Fuhrer, M. S.; Yan, J. Helicity-Resolved Raman Scattering of MoS_2, $MoSe_2$, WS_2, and WSe_2 Atomic Layers. *Nano Lett.* **2015**, *15* (4), 2526−2532.
(51) Brüesch, P. *Phonons: Theory and Experiments II: Experiments and Interpretation of Experimental Results*; Springer, 1987.
(52) Cho, G. C.; Kütt, W.; Kurz, H. Subpicosecond Time-Resolved Coherent-Phonon Oscillations in GaAs. *Phys. Rev. Lett.* **1990**, *65* (6), 764−766.
(53) Sun, Q.-C.; Mazumdar, D.; Yadgarov, L.; Rosentsveig, R.; Tenne, R.; Musfeldt, J. L. Spectroscopic Determination of Phonon Lifetimes in Rhenium-Doped MoS2 Nanoparticles. *Nano Lett.* **2013**, *13* (6), 2803−2808.
(54) Caruso, F.; Zacharias, M. Quantum Theory of Light-Driven Coherent Lattice Dynamics. *Phys. Rev. B* **2023**, *107* (5), 054102.
(55) Morita, A. *Theory of Sum Frequency Generation Spectroscopy*; Springer Berlin Heidelberg: New York, 2018.
(56) Velarde, L.; Wang, H.-F. Unified Treatment and Measurement of the Spectral Resolution and Temporal Effects in Frequency-Resolved Sum-Frequency Generation Vibrational Spectroscopy (SFG-VS). *Phys. Chem. Chem. Phys.* **2013**, *15* (46), 19970.
(57) Hahn, E. L. Spin Echoes. *Phys. Rev.* **1950**, *80* (4), 580−594.
(58) Peng, Y.-K.; Cao, Z.-Y.; Chen, L.-C.; Dai, N.; Sun, Y.; Chen, X.-J. Phonon Anharmonicity of Tungsten Disulfide. *J. Phys. Chem. C* **2019**, *123* (41), 25509−25514.
(59) Gu, X.; Yang, R. Phonon Transport in Single-Layer Transition Metal Dichalcogenides: A First-Principles Study. *Appl. Phys. Lett.* **2014**, *105* (13), 131903.
(60) Hong, J.; Hu, Z.; Probert, M.; Li, K.; Lv, D.; Yang, X.; Gu, L.; Mao, N.; Feng, Q.; Xie, L.; Zhang, J.; Wu, D.; Zhang, Z.; Jin, C.; Ji, W.; Zhang, X.; Yuan, J.; Zhang, Z. Exploring Atomic Defects in Molybdenum Disulphide Monolayers. *Nat. Commun.* **2015**, *6* (1), 6293.
(61) Huang, X.; Gao, Y.; Yang, T.; Ren, W.; Cheng, H.-M.; Lai, T. Quantitative Analysis of Temperature Dependence of Raman Shift of Monolayer WS2. *Sci. Rep.* **2016**, *6* (1), 32236.
(62) Zhang, G.; Dong, S.; Yang, C.; Han, D.; Xin, G.; Wang, X. Revisiting Four-Phonon Scattering in WS2Monolayer with Machine Learning Potential. *Appl. Phys. Lett.* **2023**, *123* (5), 052205.
(63) Bordenyuk, A. N.; Jayathilake, H.; Benderskii, A. V. Coherent Vibrational Quantum Beats as a Probe of Langmuir−Blodgett Monolayers. *J. Phys. Chem. B* **2005**, *109* (33), 15941−15949.
(64) Pandey, T.; Polanco, C. A.; Cooper, V. R.; Parker, D. S.; Lindsay, L. Symmetry-Driven Phonon Chirality and Transport in One-Dimensional and Bulk Ba3N-Derived Materials. *Phys. Rev. B* **2018**, *98* (24), 241405.

https://doi.org/10.1021/acs.nanolett.4c02787
Nano Lett. XXXX, XXX, XXX−XXX